

PCCP

Accepted Manuscript



This is an *Accepted Manuscript*, which has been through the Royal Society of Chemistry peer review process and has been accepted for publication.

Accepted Manuscripts are published online shortly after acceptance, before technical editing, formatting and proof reading. Using this free service, authors can make their results available to the community, in citable form, before we publish the edited article. We will replace this *Accepted Manuscript* with the edited and formatted *Advance Article* as soon as it is available.

You can find more information about *Accepted Manuscripts* in the [Information for Authors](#).

Please note that technical editing may introduce minor changes to the text and/or graphics, which may alter content. The journal's standard [Terms & Conditions](#) and the [Ethical guidelines](#) still apply. In no event shall the Royal Society of Chemistry be held responsible for any errors or omissions in this *Accepted Manuscript* or any consequences arising from the use of any information it contains.



Cite this: DOI: 10.1039/xxxxxxxxxx

First principles study of the atomic layer deposition of alumina by TMA/H₂O-process

Timo Weckman,^{*a} and Kari Laasonen,^a

Received Date

Accepted Date

DOI: 10.1039/xxxxxxxxxx

www.rsc.org/journalname

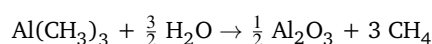
Atomic layer deposition (ALD) is a coating technology used to produce highly uniform thin films. Aluminiumoxide, Al₂O₃, is mainly deposited using trimethylaluminium (TMA) and water as precursors and is the most studied ALD-process to date. However, only few theoretical studies have been reported in the literature. The surface reaction mechanisms and energetics previously reported focus on a gibbsite-like surface model but a more realistic description of the surface can be achieved when the hydroxylation of the surface is taken into account using dissociatively adsorbed water molecules. The adsorbed water changes the topology of the surface and reaction energetics change considerably when compared to previously studied surface model. Here we have studied the TMA/H₂O process using density functional theory on a hydroxylated alumina surface and reproduced the previous results for comparison. Mechanisms and energetics during both the TMA and the subsequent water pulse are presented. TMA is found to adsorb exothermically onto the surface. The reaction barriers for the ligand-exchange reactions between the TMA and the surface hydroxyl groups were found to be much lower compared to previously presented results. TMA dissociation on the surface is predicted to seize at monomethylaluminium. Barriers for proton diffusion between surface sites are observed to be low. TMA adsorption was also found to be cooperative with the formation of methyl bridges between the adsorbants. The water pulse was studied using single water molecules reacting with the DMA and MMA surface species. Barriers for static reactions were found to be reasonably large and higher than during the TMA pulse. However, stabilizing interactions amongst water molecules were found to lower the reaction barriers and the dynamical nature of water is predicted to be of importance. It is expected that static calculations can only set an upper limit for the barriers.

1 Introduction

Atomic layer deposition is a coating technology used for the construction of various thin films. ALD is based on sequential, self-terminating gas–solid reactions. A prototype process is based on two precursors that react rapidly and violently with each other. The reaction between the precursors is forced onto the surface by alternating gas pulses while the gas-phase reactions are avoided by purging the reactor with inert gas between the pulses. Ideally each precursor pulse forms a new monolayer onto the surface. A vast majority of the ALD-processes are run at temperatures higher than 400 K. The choice for the precursors is therefore crucial for the process as there should be no reactions amongst the precursors themselves in order for the adsorption process to be self-terminating. The self-limiting nature of the adsorption in ALD enables a highly uniform and conformal deposition of a material with thickness control at the atomic level.^{1–3}

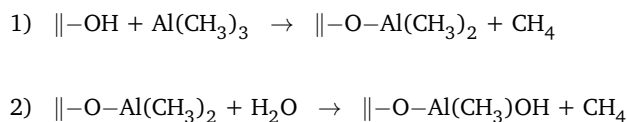
The trimethylaluminium–water-process is perhaps the most studied ALD-process. Because of the ideally self-terminating nature of the adsorption process and inertness of the reaction by-product methane, the TMA/H₂O-system is considered as a model process for ALD^{3,4} and is worth a careful study. However, only few theoretical studies have been published hitherto and most of the research concerning the process has been experimental work. Here we try to bridge this gap by revisiting some of the results previously published in the literature and also present reaction pathways for the initial reactions in the process.

The produced thin film, aluminum oxide (Al₂O₃), is an important dielectric material with a large band gap of 9 eV and moderate permittivity. Its various commercial applications include flat-screen electroluminescent displays, protective coating, read/write heads, DRAM and it has been considered as a gate dielectric in complementary metal–oxide–semiconductors, CMOS^{5–8}. The total reaction of the process is

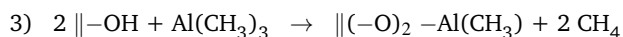


^aAalto University, Kemistintie 1, Espoo, Finland.; E-mail: timo.weckman@aalto.fi

This overall reaction is often divided into two parts, one "half-reaction" for the TMA-pulse and another one for the water-pulse (surface is described here with a \parallel)⁴



In addition to the straight-forward ligand-exchange reaction in equation (1), a reaction simultaneously with two hydroxyl groups has also been proposed⁹



TMA has also been observed to adsorb dissociatively onto the oxygen bridges on the surface.⁴

Previously only few computational studies considering the TMA/H₂O-system has been presented, focusing mainly on mechanisms (1) and (2). The first publications on the growth of Al₂O₃ thin films was done using cluster models^{10,11} consisting of only about a dozen atoms. Few papers^{12,13} using the periodic slab model with gibbsite-like Al(OH)₃-surface describing the hydroxylated alumina have been published.

As alumina is almost always covered with either dissociated or molecularly adsorbed water, hydroxylation is of great importance for aluminas surface chemistry. For example the growth-per-cycle (GPC) of the TMA/H₂O-process has been observed to be linearly dependent on the hydroxylation of the surface⁴. This hydroxylation of the alumina surface has been taken into account in the computational studies using a gibbsite-like Al(OH)₃ surface structure. However, this proposed model by Elliott *et al.*¹⁴ neglects the finite temperature effects of the hydroxylation. A more comprehensive study of the surface composition by Lodziana *et al.*¹⁵ shows that the gibbsite-like surface exists only under large water partial pressures and low temperatures (< 400 K) and is not thermodynamically stable in the process conditions (typical pulse conditions: $P = 2$ Pa, $T = 450$ K). In low pressures the surface consists of dissociatively adsorbed water which changes the surface geometry. The surface structure is not planar as is the case with gibbsite-like surface, but dissociated water introduces two hydroxyl groups, one being higher than the other. This has large effects on the previously reported reaction mechanisms and energetics.

Here we present detailed energetics of the initial reaction pathways on the hydrated surface during both the TMA and the water pulses and compare the results to the previously used gibbsite-like surface model. From these results the energetics at a finite temperature and pressure are constructed and kinetic parameters for the reactions are computed, allowing the course of the surface process to be extrapolated.

2 Computational methods

2.1 Technical details

The reaction pathways were studied using self-consistent density functional theory as implemented in GPAW¹⁶. The exchange and correlation part of the total energy was treated with gradient corrected Perdew–Burke–Ernzerhof functional¹⁷ using grid spacing of 0.2 Å. A van der Waals -correction on top of the PBE functional was used as proposed by Tkachenko and Scheffler¹⁸. The k-points sampling of the reciprocal space was done using $2 \times 2 \times 2$ Monkhorst–Pack grid for bulk calculations and $2 \times 2 \times 1$ for the surface calculations. All geometry optimizations were carried out to gradients smaller than 0.05 eV/Å. Partial charge analysis was conducted from the electron density with a Bader analysis¹⁹.

Free energies of the reaction pathways were estimated in the ideal gas limit. The translational entropy of the gaseous molecules was estimated using the Sackur–Tetrode equation

$$S_{trans} = R \left[\ln \left[\left(\frac{2\pi M k_B T}{h^2} \right)^{3/2} \frac{k_B T}{P} \right] + \frac{5}{2} \right] \quad (1)$$

where P is the pressure of the gaseous component and M is the mass of the molecule. The rotational entropy was approximated with the rigid rotor -model

$$S_{rot} = R \left[\ln \left[\left(\frac{8\pi^2 k_B T}{h^2} \right)^{3/2} \frac{\sqrt{\pi I_A I_B I_C}}{\sigma} \right] + \frac{3}{2} \right] \quad (2)$$

where σ is the symmetry number corresponding to the molecule (6 for TMA, 12 for CH₄ and 2 for H₂O) and I_A , I_B and I_C are the principal moments of inertia. Bond vibrations were treated as harmonic oscillations:²⁰

$$S_{vib} = R \sum_i \left[\frac{h\omega_i}{k_B T (e^{h\omega_i/k_B T} - 1)} - \ln(1 - e^{-h\omega_i/k_B T}) \right] \quad (3)$$

To reduce the computational burden associated with vibrational calculations on the solid surface the vibrations on the surface were restricted only to the top layer and bulk modes were assumed to remain unchanged. To avoid erroneous contributions from low frequency modes corresponding to internal rotations, the low frequency modes were omitted from the vibrational partition function. Low frequency modes were defined as modes corresponding to wavenumber less than 209 cm⁻¹ which corresponds to 300 K.

The kinetic model was constructed from the elementary steps studied. Reaction rate coefficients for the kinetic equations were calculated using the Eyring equation²¹ in the harmonic approximation:

$$k_i = \frac{k_B T}{h} e^{-\frac{\Delta G_i^\ddagger}{k_B T}} \quad (4)$$

where h is the Planck constant and ΔG_i^\ddagger is the Gibbs activation free energy for the reaction pathway i .

The minimum energy paths (MEP) for transition states were found using the nudged elastic band method²² where the potential energy surfaces first-order saddle point for transition from initial to final state is found by setting consecutive images of the system along the reaction path. These replicas are connected to

each other by a harmonic force and relaxed along the MEP. The initial guess of the path was created by interpolating the configurations between the initial and final geometries. Transition state was found using the so-called climbing image method with alternating force constants.

2.2 Substrate models

During ALD growth amorphous alumina is deposited onto the substrate. However, amorphous structure is difficult to simulate *ab initio*, so a α -Al₂O₃ crystalline structure was chosen as in previous studies^{12,13,23,24}. The α -Al₂O₃ (0001) surface has been studied both experimentally and theoretically²⁵⁻²⁹ and the Al-terminated surface has been shown to be the most stable surface of α -Al₂O₃.

The surface was modelled using the slab model with periodic boundary conditions imposed. The thickness of the slab was one unit cell with a vacuum of about 9 Å on both sides of the slab. The bottom layers were constrained for the calculations. The surface cells consisted of 2 × 2 unit cells with surface area of 0.82 nm².

The surface hydroxylation was taken into account using dissociatively adsorbed water surface presented by Lodziana *et al*¹⁵. The resulting hydrated surface has a hydroxyl group coverage of about 16 μmol m⁻² that is very close to the experimental value of 15 μmol m⁻²³⁰. The gibbsite-like surface is constructed by replacing the top-most aluminium atoms with three hydrogen atoms. Hydroxyl concentration on the gibbsite-like surface is about 25 μmol m⁻². The previous study by Elliott and Greer¹² using gibbsite-like surface was also repeated for comparison.

The adsorption energy for the dissociatively adsorbed water molecules were calculated as an average over all the adsorbed water molecules in the monolayer,

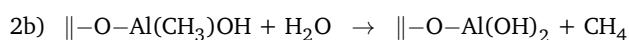
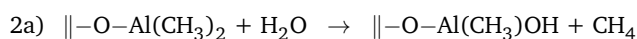
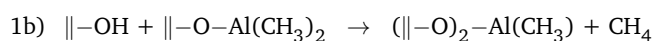
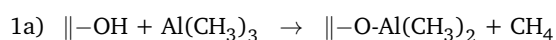
$$E_{ads} = \frac{E_{slab} - E_{Al_2O_3} - NE_{H_2O}}{N} \quad (5)$$

where $E_{Al_2O_3}$ is bare aluminium slab or the previously filled monolayer and E_{H_2O} is a single water molecule in a vacuum.³¹

3 Results

Both the TMA and water pulses were studied. The TMA adsorption and subsequent ligand-exchange reactions were studied on the hydrated and on the gibbsite-like surface. The water pulse was studied using static calculations with few water molecules.

The main mechanisms studied can be summed up by the following reaction equations:



Equations 1a, 1b and 1c represent reactions during the TMA pulse and 2a, 2b and 2c reactions during the water pulse. Some additional calculations were also done, e.g. the effect of several adsorbants during the TMA pulse, and will be discussed in the text. The main reaction mechanisms were treated with a vibrational analysis and the free energies for these reactions were calculated.

In the reaction 1a the TMA is decomposed into dimethylaluminium (DMA) surface species and in the second reaction reacts with the surface even further to produce a monomethylaluminium (MMA). These two products are taken as the starting points for the water pulse. Water pulse reactions were studied with only a single TMA molecule in a 2 × 2 unit cell representing low TMA coverage.

3.1 Alumina – bulk and surface

The bulk oxide model was optimized using DFT by scanning the potential energy surface by changing the lattice vectors and keeping the lattice angles constant. The optimized cell parameters were found to be $a = b = 4.762$ Å and $c/a = 2.760$ in close agreement with both experiment³² and other theoretical studies^{12,15}.

The heat of adsorption for water was found to be in great agreement with the results previously reported (see table 1). The addition of the van der Waals -correction somewhat increases the adsorption energy. The adsorption energy lowers considerably after the adsorption of the first monolayer and the additional monolayers are only loosely bound.

Adsorbed water produces surface structure that has two distinct hydroxyl groups (see figure 1). The higher hydroxyl groups are formed from the water molecule and the lower is formed from the dissociated hydrogen that bonds to a surface oxygen. TMA adsorption is possible only onto to higher hydroxyl group due to steric effects.

The gibbsite-like surface was constructed by replacing the top Al-atoms with three hydrogen atoms. Two of these hydrogens orient vertically and one horizontally with respect to the surface (figure 2). Adsorption to the horizontal group is preferred due to the possible Lewis acid-base reaction between the TMA and the oxygens lone pair of electrons, but adsorption to the vertical group was also found to be possible.

The differences in the surface geometries cause a difference in the electronic structures between the two models. There is however only small difference in the bond lengths and partial charges between the two surfaces. All the Al–O bonds in the bulk phase are 1.9-2.0 Å and partial charges 2.5 and -1.6 for aluminium and oxygen, respectively. On the gibbsite-like surface Al–O bonds are close to the bulk values but on the hydrated surface they are slightly shorter (1.7 Å). Partial charges on the surface atoms are slightly smaller than in the bulk on both surfaces.

Table 1 The adsorption energies for water with different surface coverages given in eV per water molecule. The asterisk denotes dissociative adsorption. The monolayer is defined as a water molecule per a 1×1 unit cell which gives a surface hydroxide concentration of $16 \mu\text{mol m}^{-2}$ for 1 ML coverage.

	$\frac{1}{4}$	$\frac{1}{2}$	1	2	3
Lodziana <i>et al.</i> , PW91-functional	-1.379 *	-1.517 *	-1.516 *	-0.780	-0.494
This work, PBE	-1.202 *	-1.256 *	-1.383*	-0.607	-0.378
This work, PBE + vdW	-1.336 *	-1.563 *	-1.487*	-0.956	-0.409

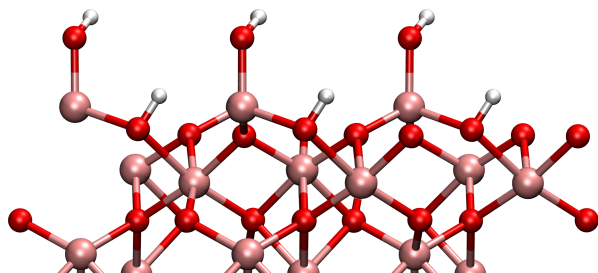


Fig. 1 Side-view of the hydrated surfaces formed from dissociatively adsorbed water. Two kinds of hydroxyl groups are present, the higher group formed from the water molecule and the lower one formed with the dissociated hydrogen and surface oxygen. A monolayer coverage is achieved when four water molecules adsorb onto a 2×2 cell. Only three molecules are visible from this view due to overlap.

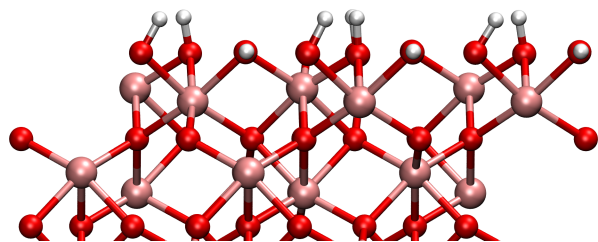


Fig. 2 Side-view of the gibbsite-like surface. Stoichiometric gibbsite-layer is formed when the top aluminium atoms are replaced with three hydrogen atoms. Gibbsite-like surface gives two vertical and one horizontal hydroxyl groups per unit cell.

3.2 Reactions during the TMA pulse

3.2.1 TMA adsorption and first dissociation

On the hydrated surface the TMA adsorption takes place on one of the higher hydroxyl groups. Adsorption to the lower hydroxyl groups is blocked by steric interaction. The adsorption was found to be exothermic with adsorption energy of -1.13 eV. Any translational motion between adsorption sites on the surface is blocked by a diffusion barrier of 0.88 eV.

A straight-forward ligand-exchange reaction with the adsorbent hydroxyl groups was assumed to take place as in mechanism 1a. The TMA's methyl group forms a methane molecule with the proton of the hydroxyl group and desorbs into the gas phase. Barrier for this ligand-exchange reaction was found to be only 0.35 eV with reaction energy of -0.70 eV.

The same mechanism was also studied on the gibbsite-like surface. Just as previously shown by Elliott and Greer^{12,13}, the TMA most favourably adsorbs onto the horizontal hydroxyl group. The

adsorption energy to the horizontal group was -1.60 eV, considerably more exothermic than on the hydrated surface. However, we found that for the ligand-exchange reaction TMA preferably bonds to a vertical hydroxyl group where the proton is more accessible. Adsorption energy directly to the vertical hydroxyl group would be -1.52 eV. The reaction barrier for the reaction is 0.69 eV in agreement with the previously reported result of 0.9 eV by Elliott and Pinto¹³. At the end of the reaction DMA is coordinated to two oxygens which makes the configuration very stable. The overall reaction energy after the desorption of methane was -0.88 eV. The adsorbed TMA on the two different surfaces is illustrated in figure 3. The transition and final states on both surface models are illustrated in figure 4.

While TMA adsorbs exothermically on both surfaces, the adsorption energy on the gibbsite-surface is 0.5 eV more negative than on the hydrated surface. Yet, there is very little difference between the adsorption bond lengths (Al–O bond 2.04 Å and 2.02 Å on the hydrated and gibbsite surface, respectively). The TMA is more distorted from its gaseous planar structure on the gibbsite-like surface probably because of the stronger Al–O adsorption bond. The C–Al–C-dihedral changes from the planar 180° to about 240° on the adsorption to the gibbsite surface, which is considerably more than the distortion on the hydrated surface where the dihedral is only about 218° . The distortion can also be partially due to steric interactions between the methyl groups and the neighbouring hydroxyl groups. The distance between the methyl and hydroxyl groups is 0.5 Å shorter on the gibbsite-surface than on the hydrated surface.

While there is little difference in the initial structures between the two surface models, the final states are very different. On the hydrated surface the aluminium is bonded only to one oxygen and hence the Al–O bond is shorter (1.71 Å) than on the gibbsite surface (1.92 and 1.81 Å) where aluminium is twice coordinated. The larger coordination on the gibbsite surface leads to a surprisingly small difference in the overall reaction energy. Just as in the adsorption of the TMA, the DMA resulting from the reaction is also more distorted on the gibbsite than on the hydrated surface. C–Al–C angle is closer to the triangular geometry on the hydrated surface (121.6°) than on the gibbsite surface (100.8°) where the angle deviates severely from the planar configuration.

Considering the difference in the activation energies, the difference in the bond lengths during the reaction is surprisingly small. The Al–O and Al–C bonds are slightly (0.03 – 0.04 Å) longer in the transition state on the gibbsite surface. From the partial charges it can be seen that the reaction takes place between the negative methyl group (ca. -0.8 charge on the carbon atom) and a

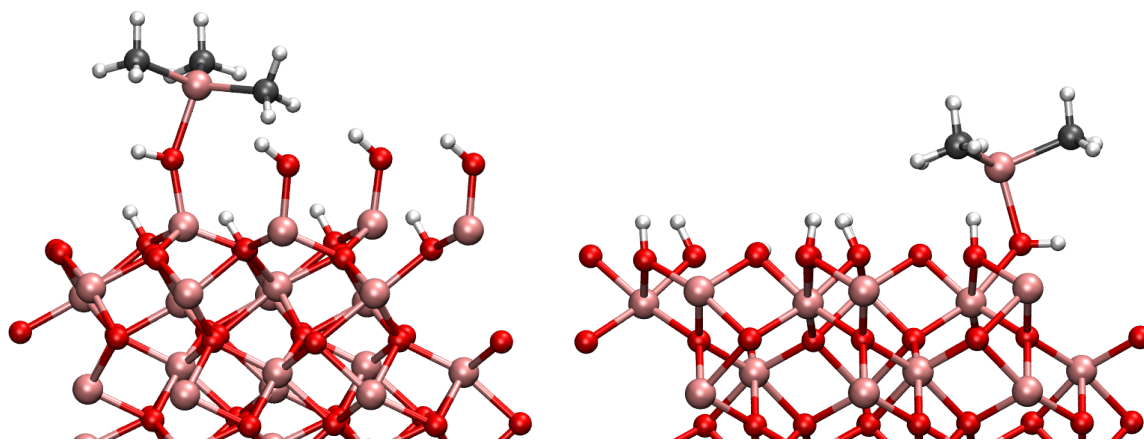


Fig. 3 Adsorbed TMA on the hydrated surface (left) and on the gibbsite surface (right). Brown, red, black and white spheres represent aluminium, oxygen, carbon and hydrogen, respectively. The TMA is more distorted from its planar structure on the gibbsite surface than on the hydrated surface. However, the adsorption energy on the gibbsite-surface is 0.5 eV more exothermic than on the hydrated surface. There is no differences in the adsorption bond lengths between the two surface models.

positively charged proton of the hydroxyl group.

The effect of the surface coverage to the initial reaction on the hydrated surface was also studied. Adsorption of another TMA next to the DMA was found to lead to an increase in the adsorption energy. The adsorption energy of the second TMA is -1.32 eV, slightly more exothermic than the for a single TMA. The second TMA can undergo a similar ligand-exchange reaction with the adsorbent hydroxyl group similar to the first reaction. Higher surface coverage leads to a slight increase in the activation energy. Activation energy for the second TMA was 0.45 eV with reaction energy of -0.48 eV.

Interestingly the adsorption energy for a third TMA is even more exothermic, -1.90 eV. However, with two DMAs and one TMA, the high surface coverage leads to steric interaction with the neighbouring adsorbants and raises the activation energy for the reaction to 0.72 eV. The ligand-exchange reaction becomes considerably less exothermic with reaction energy of only -0.15 eV with large surface coverage.

The cause of this cooperative adsorption is the formation of methyl-bridges between the adsorbants, illustrated schematically in figure 5. This cooperative adsorption might be of importance during the adsorption process and may possible lead to an island-like growth of the adsorption layer. Also, the formation of methyl-bridges between the aluminium atoms can have great stabilizing effect when considering the structure of the surface at the end of the TMA pulse.

3.2.2 Second dissociation

Experiments show that the amount of adsorbed aluminium is linearly dependent on the surface hydroxylation and that the methyl concentration of the surface remains approximately constant after a TMA pulse, ca. 5-6 methyl groups per nm^2 . Thus, the Al:Me-ratio also decreases at high hydroxyl concentrations and at OH-concentration of about $15 \mu\text{mol m}^{-2}$ the ratio is 1.5. This suggests that the surface is mainly composed of dimethylaluminium and monomethylaluminium.^{4,9}

Therefore it is to be expected that DMA undergoes further

ligand-exchange reactions on the surface, i.e. mechanisms **1b** and **1c**. Several possible pathways for the second reaction were studied and the lowest reaction barrier was found for direct reaction with a neighbouring hydroxyl group (see figure 6). The activation energy for the reaction is 0.51 eV, slightly higher than for the reaction **1a**. The change in the activation energy is relatively small considering that the proton on the neighbouring hydroxyl group is expected to be less acidic than the proton in the reaction **1a** and that the DMA has to react with a proton several angstroms away. This requires almost linear Al-O-Al bond to bend down to 140° . In the final state the monomethylaluminium is bonded to three oxygens of three hydroxyl groups which makes the reaction extremely exothermic with respect to previous reactions with reaction energy of -1.38 eV. As the MMA bonds with three hydroxyl groups, proton-transfer between a lower hydroxyl group and a protonless higher hydroxyl group is observed.

As the ligand-exchange reactions consume protons from the surface to produce methane, the resulting bare oxygen sites make the surface even more basic. The adsorption of a TMA to the bare oxygen around the MMA is exothermic with -1.65 eV which is 0.5 eV more exothermic than adsorption onto a hydroxyl group. Addition of another TMA next to the same MMA causes steric interaction between the adsorbants leading to a weak adsorption bond for the second TMA.

Adsorption to the hydroxyl group next to the MMA is also possible. Adsorption of a TMA to the hydroxyl group that is bonded to the MMA is exothermic with -1.15 eV, same as for an isolated hydroxyl group. The activation energy for the ligand-exchange reaction with this hydroxyl group is however considerably higher than for the initial reaction, over 1 eV with reaction energy of -1.11 eV, making the hydroxyl group practically inert. Adsorption of a TMA was observed not to considerably effect the energetics of the MMAs reaction with a hydroxyl group i.e. the third dissociation.

The DMA on the gibbsite-like surface is coordinated to two oxygens and is hence constrained to its location. Only a reaction with

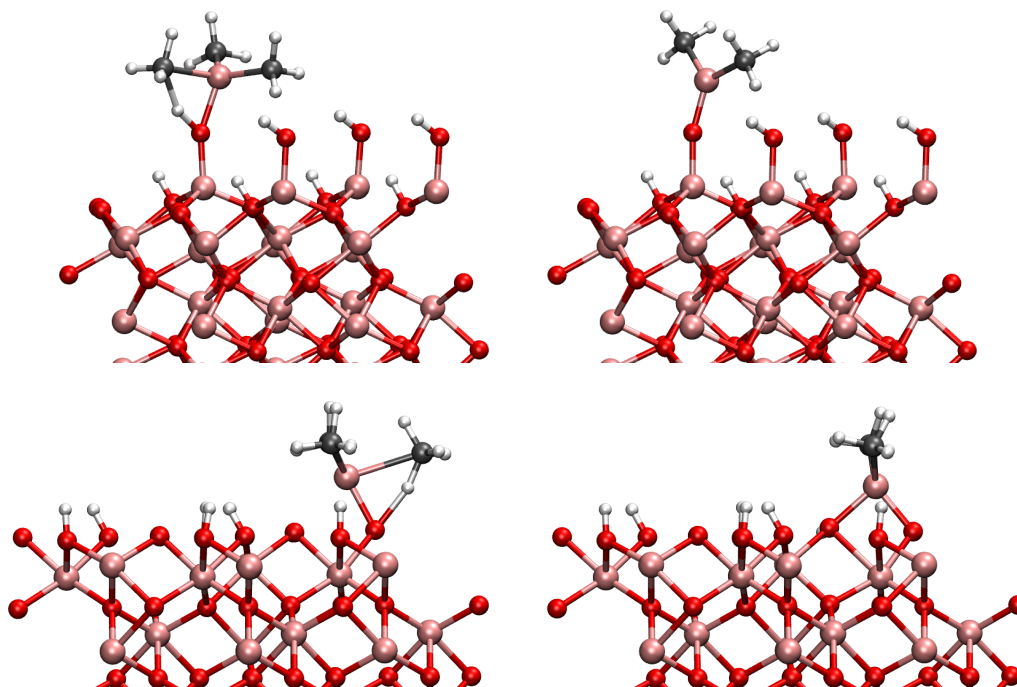


Fig. 4 On the left is the transition state for the initial reaction on the hydrated surface (top) and on the gibbsite-like surface (below). The TMA is less hindered on the hydrated surface and the transition state is more easily reached. On the right side is the final state after the ligand-exchange reaction. The DMA is coordinated to one oxygen on the hydrated surface but twice coordinated on the gibbsite-like surface. On the hydrated surface, adding another TMA onto a neighbouring hydroxyl group was found to slightly increase activation energy of the reaction but also to significantly increase the adsorption energy.

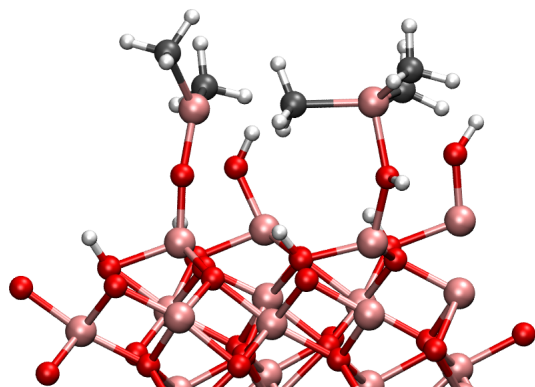


Fig. 5 An example of a bridged structure. The bridged structure stabilizes the adsorbed structure and increases the adsorption energy of the TMA.

the neighbouring hydroxyl group is possible. The activation energy for a reaction with the closest neighbour was calculated to be 0.72 eV which is slightly higher than in the first reaction. This results in a stable monomethylaluminium coordinated to three oxygens. The reaction is exothermic with reaction energy of -1.15 eV.

3.2.3 Third dissociation

The monomethylaluminium is coordinated to three oxygens on the surface and is therefore extremely rigid. The only plausible pathway for the MMA to react is to receive a proton from

one of the hydroxyl groups (see figure 7). However, due to the rigid structure of the MMA the activation energy for the ligand-exchange reaction becomes high. This reaction mechanism leads to densification of the surface that is not observed in the other mechanisms. The activation energy for the reaction is 1.05 eV with reaction energy of -0.44 eV.

Different mechanisms were studied for reactions **1b** and **1c**. Some of these mechanisms involved proton transfer from one hydroxyl group to another. The barriers for proton diffusion on the surface amongst the lower and higher hydroxyl groups can be estimated to be around 0.5 – 0.6 eV with negligible reaction energies.

3.3 Reactions during water pulse

After the TMA has saturated the surface, the gas-phase is cleaned with inert gas and a water pulse is introduced to the system. Here we have studied the mechanisms for the water pulse using static calculations similar to other previous studies^{10,33}. An accurate estimation of the surface structure after the TMA pulse is beyond the scope of this work. Therefore, the final states of reactions **1a** (DMA) and **1b** (MMA) were taken as the initial configurations for the water pulse mechanisms. The water pulse reactions studied are schematically represented by the equations 2a–c.

3.3.1 Dimethylaluminium and water

Just like the TMA, the DMA is a Lewis-acid and is therefore an ideal adsorption site for Lewis-basic water molecules. The ligand-

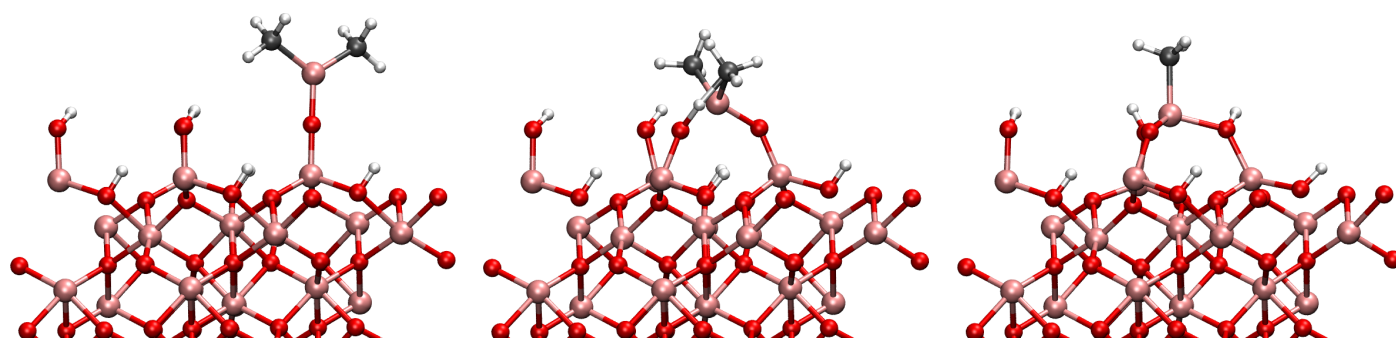


Fig. 6 The initial, transition and final states in the second ligand-exchange reaction. The initially linear Al–O–Al bond needs to bend from 180° angle down to 140° in order to reach the transition state. Notice that a proton is transferred to the adsorbent oxygen after the transition state.

exchange mechanism between the DMA and water is straightforward, the water adsorbs to the DMA and donates a proton to the methyl-ligand. However, depending on the orientation of the water molecule, the water molecule can form hydrogen bonds with the other hydroxyl groups. This considerably increases the adsorption energy but also constraints the water molecule which in turn increases the reaction barrier (see figure 8). For the hydrogen bonded water the adsorption energy is -1.50 eV and the barrier for the ligand-exchange reaction is 1.01 eV. For the non-hydrogen bonded water molecule the adsorption energy and reaction barrier are -0.64 eV and 0.44 eV, respectively. The two mechanisms are similar and result in a monomethylaluminium hydroxide. Reaction energies for the two mechanisms are -0.02 eV (hydrogen bonded) and -0.61 eV (non-bonded).

The resulting monomethylaluminium hydroxide can further react with water into an aluminium dihydroxide. Just as in the previous mechanism **2a**, the adsorption energy depends whether or not the water forms hydrogen bonds with the hydroxyl groups. An adsorption energy of a hydrogen bonded water molecule to the MMA-OH is -1.66 eV and for a non-hydrogen bonded the adsorption energy is -1.13 eV. The difference in the reaction barrier between these two configurations is smaller than in the mechanism **2a**. Reaction barriers and energies for the hydrogen bonded and non-bonded mechanisms are 1.18 eV, 0.29 eV and 0.67 eV, -0.28 eV, respectively. The reaction path for the non-hydrogen bonded mechanism is illustrated in figure 9.

3.3.2 Monomethylaluminium and water

The structure of the monomethylaluminium is very different from the DMA. The aluminium is "shielded" by the surrounding oxygens and it was found that the closed structure made it impossible for a single water molecule to remove the methyl-ligand from the MMA. A short *ab initio* molecular dynamics simulation with several water molecules suggested that a water molecule might first break the MMA structure from three oxygen coordinated to a two coordinated one. This structure could then react with another water molecule. We have here studied the mechanism **2c** with several water molecules and labelled them as **2c_{w1}**, **2c_{w2}** and **2c_{w3}** depending on the amount of water molecules within the mechanism.

The attack by a water molecule to the MMA aluminium is illustrated in figure 10. The adsorption energy of the water molecule to the surface is -0.64 eV which is quite small when compared to the adsorption energies on the DMA. In the reaction path studied (mechanism **2c_{w1}**), the water molecule was observed to donate one of its protons to a neighbouring hydroxyl group and bonding to the MMA as a hydroxyl group. The barrier for this reaction is small, only 0.26 eV with exothermic reaction energy of -0.62 eV. After the reaction the MMA is no longer blocked and there is enough space for another water molecule to attack.

When the MMA structure is opened, an attack by a water molecule from the opposite side is possible. This mechanism is denoted **2c_{w2}** since it now involves two water molecules. The re-

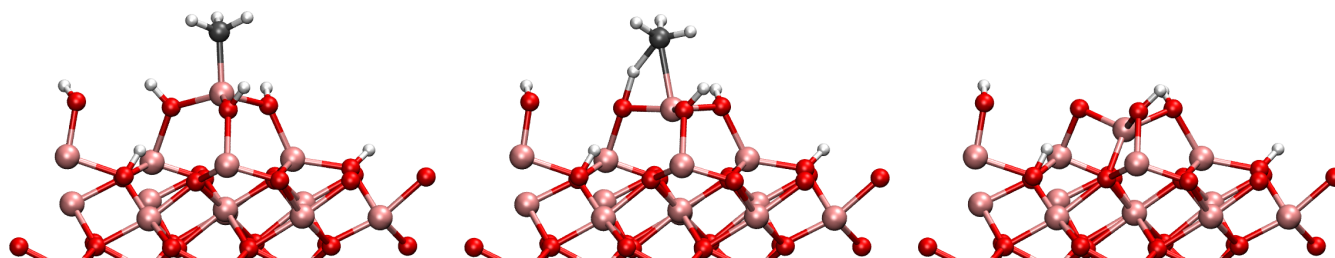


Fig. 7 The initial, transition and final states for the proposed third ligand-exchange reaction. The final dissociation of the TMA leads to densification of the surface which is not observed in the other reaction pathways. However, the ligand-exchange reactions are predicted to stop at the second dissociation due to the high barrier for the third reaction.

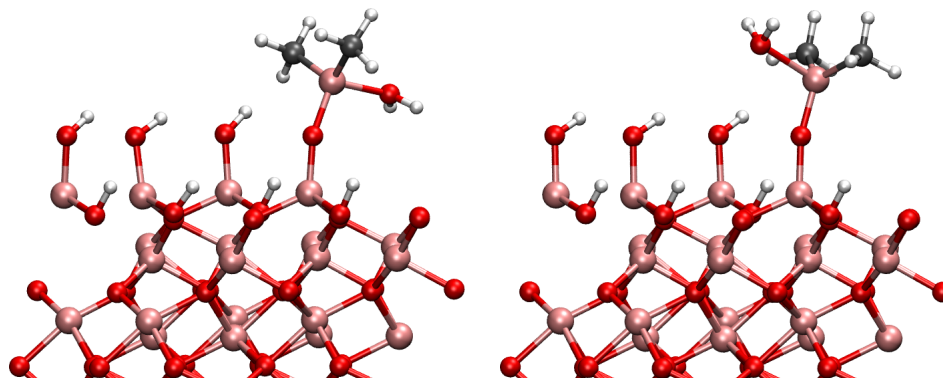


Fig. 8 On the left the water molecule has formed hydrogen bonds with the surface hydroxyl groups (with periodic image). This increases the adsorption energy considerably but also increases the activation energy of the reaction. On the right no hydrogen bonds are formed and reaction barrier is much lower.

action was found to have a barrier of 0.63 eV and reaction energy of -1.07 eV. However, also a mechanism containing an additional water molecule was tested. This was found to considerably lower the reaction barrier (mechanism $2c_{w3}$), illustrated in figure 11. The barrier was brought down to 0.39 eV with increased reaction energy of -1.61 eV. The adsorption energy of a water molecule was calculated to be -0.72 eV for both mechanisms $2c_{w2}$ and $2c_{w3}$.

3.4 Free energy surface of reaction pathways

In order to improve the zero temperature calculations and make the energetics comparable to a real system, the free energy profiles of the reaction pathways were calculated using equations (1),(2) and (3). For gaseous species translational, rotational and vibrational contributions were considered. For surface species only vibrational contributions were included.

To avoid inclusion of internal rotational modes in the vibrational entropy, high frequency modes for which $\tilde{\nu} \leq 209$ cm^{-1} were omitted. Free energies on the pathways were calculated in temperatures 298.15 K and 450 K with TMA pressure of 2 Pa.

4 Discussion

4.1 Reaction energetics of the TMA pulse

We have studied TMA adsorption and subsequent surface reactions on a realistic hydrated surface model and compared our results with previously reported study on a gibbsite-like surface model. The reaction energetics and the zero-point energy corrected values for the TMA pulse are presented in table 2. Previously presented results were also replicated due to differences in computational methods. Our reaction energetics on the gibbsite-surface are similar to previously reported results with the exception of the adsorption energy which was estimated to be 0.6 eV more exothermic than previously stated in the literature. This is mainly caused by the implemented van der Waals -correction that was not included in the previous simulations.

Our results show that TMA adsorbs to the hydroxylated alumina surface exothermically with adsorption energy of -1.13 eV. Adsorption energy on the hydrated surface is 0.5 eV less exothermic than on the gibbsite-like surface. Addition of another TMA was found to increase the adsorption and activation energies slightly. This effect was further increased with the inclusion of a third TMA indicating a cooperative effect among the adsorbants. The additional TMA is able to form methyl-bridges with the neighbouring DMAs which considerably increases the adsorption en-

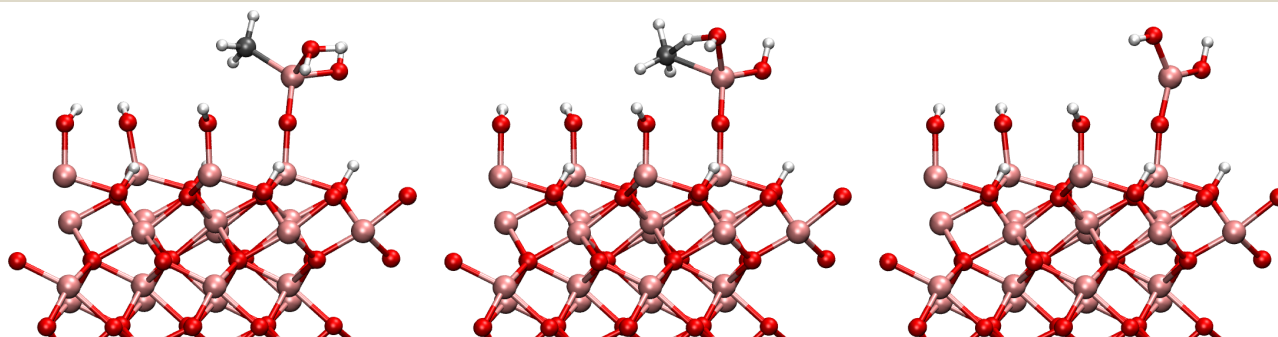


Fig. 9 The initial, transition and final states for the reaction between water molecule and a monomethylaluminium hydroxide. The illustrated mechanism depicts a non-hydrogen bonded configuration.

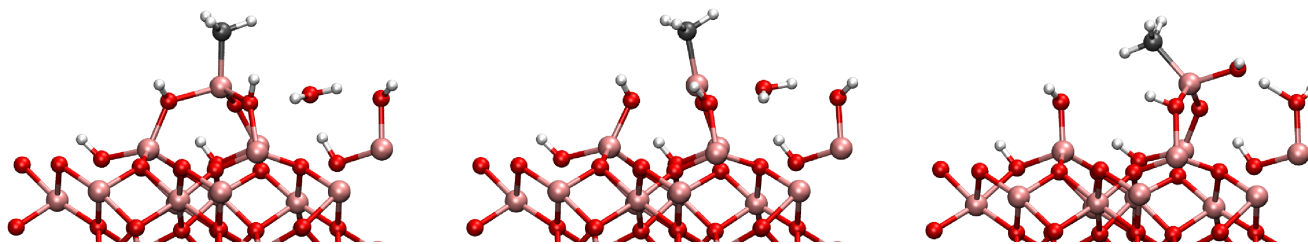


Fig. 10 The MMA is not able to react with a water molecule. However, it is possible for a water molecule to break down the inert and closed structure of the MMA.

ergy. However, the activation energy for the ligand-exchange reaction also increases due to steric effects as the surface becomes crowded.

On the surface the TMA can go through three ligand-exchange reactions with intermediate products dimethylaluminium (DMA) and monomethylaluminium (MMA). Reaction barriers for these ligand-exchange reactions were found to be considerably lower than previously reported. For the removal of the first methyl-ligand on the hydrated surface the reaction barrier was only 0.35 eV. As the surface reactions progress the methyl-group removal was found to become less favourable. For the second ligand activation energy was found to be 0.51 eV and for the final methyl the barrier rose to 1.05 eV. All the reactions were exothermic. For the first two ligand-exchange reactions the reaction energies are -0.70 eV and -1.38 eV, respectively. The reaction energy increases considerably as the reacted MMA becomes three times coordinated with oxygen. The MMA is however very rigid, resulting in high reaction barrier and low reaction energy of -0.44 eV. Due to the high reaction barrier of the last reaction step, it is probable that at the end of the TMA pulse the surface consists mainly of MMA species.

The production of MMA consumes protons from the surface creating bare oxygen sites to which the TMA adsorption is stronger than on a hydroxyl group. For example, adsorption energy to a bare oxygen next to an MMA was -1.65 eV. Here the TMA can react with the protons from the lower hydroxyl groups. We estimate the barrier for the proton transfer between an already reacted higher hydroxyl group and a lower hydroxyl group to be of the order of $0.5 - 0.6$ eV. However, preliminary results show that barriers for the ligand-exchange between the surface and a TMA adsorbed next to an MMA are high.

As an extreme case, adsorption of a TMA to a bare alumina

surface is -2.56 eV. TMA dissociates readily on the bare surface and it could be possible that the adsorbed TMA dissociates on the surface if there are no protons are left on surface to react with.

The barriers of the surface reactions on the hydrated surface are considerably lower than on the gibbsite-like surface previously used in the literature. The difference in the activation energies for the first two ligand-exchange reactions are 0.36 eV and 0.27 eV. However, this difference is lowered to 0.19 eV and 0.09 eV, respectively, when the zero-point energies are included.

One of the main differences between the hydrated surface model and the previously studied gibbsite model is the geometry of the surface. The hydrated surface has hydroxyl groups in two different planes while the gibbsite-surface is entirely planar. The adsorbed TMA is less hindered by the neighbouring hydroxyl groups and can more easily reach the transition state on hydrated surface. On the gibbsite-like surface the planar structure leads to interactions with the neighbouring hydroxyl groups and makes the TMA more rigid. However, the resulting DMA is twice coordinated to oxygen on the gibbsite-like surface leading to a larger reaction energy.

4.2 Reaction energetics of the water pulse

Reactions during the water pulse were studied using static simulations with one to three water molecules. The final states of DMA and MMA obtained from the TMA pulse calculations were used as the initial configurations for the water pulse. Results of these reaction energetics are presented in table 3.

Water adsorption energies were sensitive depending whether or not hydrogen bonds were formed with surface hydroxyl groups. Formation of hydrogen bonds considerably increases the adsorption energy but also increases the barrier for the ligand-exchange reactions with DMA and MMA-hydroxide. Adsorption

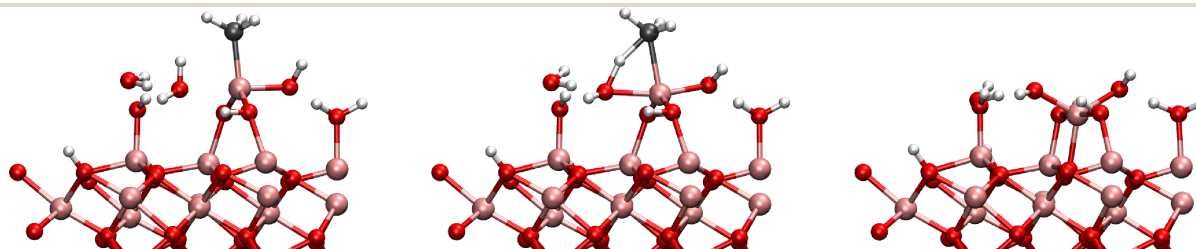


Fig. 11 Reaction between the MMA and two water molecules. The second water molecule stabilizes the transition and final states lower the activation energy by 0.24 eV.

Table 2 Energies on the potential energy surface of the TMA pulse. Energy differences are taken with respect to the initial stage of the surface reaction. Adsorption energies are for a single adsorbed molecule. ZPE-corrected values are given in parenthesis. Values are given in eV.

Mechanism		E_{ads}	E_a	ΔE
Elliot & Pinto ¹³				
Reaction 1a		-0.9	0.9	-1.2
This work				
Reaction 1a	first TMA	-1.13 (-0.99)	0.35 (0.32)	-0.70 (-0.73)
	second TMA	-1.32 (-1.14)	0.45 (0.50)	-0.48 (-0.56)
	third TMA	-1.90 (-1.70)	0.71 (0.70)	-0.15 (-0.24)
	Gibbsite-surface	-1.52 (-1.22)	0.69 (0.51)	-0.88 (-0.99)
Reaction 1b		–	0.51 (0.38)	-1.38 (-1.49)
	Gibbsite-surface	–	0.72 (0.59)	-0.88 (-1.01)
Reaction 1c		–	1.05 (0.88)	-0.44 (-0.59)

to the DMA was of the order of chemisorption (–1.50 eV) with hydrogen bonds and almost of the order of physisorption (–0.64 eV) when no hydrogen bonds were formed. However, hydrogen bonded water molecules are not free to react which results in a higher reaction barrier. With hydrogen bonds the barrier rose to 1.01 eV for the ligand-exchange mechanism with the DMA while the non-hydrogen bonded water molecule had barrier of only 0.44 eV for the same reaction.

Difference in the adsorption energies with hydrogen bonded and non-bonded water molecules was smaller (–1.66 eV vs. –1.13 eV) in the case of MMA-hydroxide. However, the formation of hydrogen bonds has a clear difference in the reaction barriers. The hydrogen bonded configuration has a barrier of 1.18 eV while the non-bonded system has a smaller barrier of 0.67 eV.

The MMA acquired from the TMA pulse calculations was found to be inert to a direct attack by a water molecule. A possible reaction pathway was found by sampling different configurations by *ab initio* molecular dynamics involving several water molecules. A water molecule was found to be able to form a bond with the MMA aluminium and opening up the MMA's closed structure. Another water molecule can then attack the MMA and undergo a ligand-exchange reaction similar to the one with the DMA and MMA-hydroxide in reactions **2a** and **2b**.

The interactions between water molecules were found to play an important role. A barrier for the adsorption of the water onto the MMA was 0.26 eV. However, the adsorption happened spontaneously during a dynamical simulation with ten or so water molecules so water–water-interactions can lower this barrier even further. Also, an addition of another water molecule next to the attacking water molecule in reaction pathway **2c** was able to lower the reaction barrier 0.2 eV. The importance of the dynamic nature of water during the surface reactions in an ALD-process has previously been pointed out by Mukhopadhyay *et al.*³³.

4.3 Energetics at a finite temperature

In order to investigate the results at the process conditions, finite temperature was included in our energetics. Entropic contributions were estimated using equations (1)-(3). Gibbs free energies for the reaction pathways in temperatures 298.15 K and 450 K are presented in tables 4 and 5.

The adsorption energies are dominated by the translational and rotational entropies of the gaseous molecules due to high temperature and especially low pressure. The entropy change in the adsorption of TMA at 298.15 K is 1.21 eV and at 450 K is 1.94 eV, which leads to positive free energies for adsorption above room

Table 3 Energies on the potential energy surface. Energy differences are taken with respect to the initial stage of the surface reaction itself. Values are given in eV. Adsorption energies are for a single adsorbed molecule. ZPE-corrected values are given in parenthesis.

Mechanism		E_{ads}	E_a	ΔE
Reaction 2a	(hydrogen bonded)	-1.50 (-1.27)	1.01 (0.84)	-0.02 (-0.26)
	(non-bonded)	-0.64 (-0.47)	0.44 (0.31)	-0.61 (-0.81)
Reaction 2b	(hydrogen bonded)	-1.66 (-1.44)	1.18 (1.08)	0.29 (0.20)
	(non-bonded)	-1.13 (-1.05)	0.67 (0.71)	-0.28 (-0.35)
Reaction 2c	w1	-0.64 (-0.52)	0.26 (0.26)	-0.62 (-0.65)
	w2	-0.72 (-0.63)	0.63 (0.62)	-1.07 (-1.24)
	w3	-0.72 (-0.56)	0.39 (0.25)	-1.61 (-1.65)

Table 4 Free energies of the reaction paths during the TMA pulse. Free energies are given in two temperatures, 450 K and 298 K (in parenthesis). Energy differences are taken with respect to the initial stage of the surface reaction. Adsorption energies are for a single adsorbed molecule. Values are given in eV.

Mechanism		ΔG_{ads}	ΔG_a	ΔG
Reaction 1a	first TMA	0.53 (-0.05)	0.30 (0.32)	-1.64 (-1.33)
	second TMA	0.14 (-0.23)	0.49 (0.50)	-1.51 (-1.17)
	third TMA	-0.19 (-0.77)	0.71 (0.71)	-1.27 (-0.89)
	Gibbsite-surface	0.34 (-0.26)	0.49 (0.50)	-1.95 (-1.61)
Reaction 1b		–	0.39 (0.38)	-2.43 (-2.09)
	Gibbsite-surface	–	0.56 (0.58)	-2.00 (-1.64)
Reaction 1c		–	0.92 (0.90)	-1.56 (-1.21)

temperature. While this entropic effect makes the adsorption free energy more positive, it also increases reaction energies as the methane desorption produces entropy and the free energy of the reaction steps become more negative at higher temperatures. The reaction barriers are overall quite temperature neutral showing only small deviations as a function of temperature.

The high temperature and low pressure of the process makes the adsorption the rate limiting step. Adsorption of the TMA was found to be cooperative with the formation of methyl bridges between adsorbants. On the surface the first ligand-exchange reactions are considerably faster than the adsorption rate. The adsorption rate, k_{ads} , can be approximated as the collision flux in kinetic theory of gases²¹:

$$k_{ads} = \frac{P\sigma(T, \theta)}{\sqrt{2\pi mk_B T}} A_{OH} \quad (6)$$

where the P is the pressure of the adsorbant, m is mass of the precursor molecule and A_{OH} is the "area of a hydroxyl group" taken as a reciprocal of the surface concentration of the top-most hydroxyl groups i.e. 4.89 OH/nm^2 . $\sigma(T, \theta)$ is the sticking probability of the adsorbant, which is unity at low surface coverage. The initial adsorption rate is then $k_{ads} = 4.2 \cdot 10^3 \frac{1}{s}$ per a hydroxyl group at the process conditions ($P = 2 \text{ Pa}$, $T = 450 \text{ K}$). The adsorption rate is several orders of magnitude smaller than the reaction rates for the first two surface reactions: for the reactions **1a**, **1b** and **1c** the rates at 450 K are $k_{1a} = 3.6 \cdot 10^9 \frac{1}{s}$, $k_{1b} = 4.6 \cdot 10^8 \frac{1}{s}$ and

Table 6 Reaction rate coefficients for different reaction pathways during the TMA pulse. Rate coefficients are given in temperatures 298 K and 450 K.

Mechanism	$k_{298}/\frac{1}{s}$	$k_{450}/\frac{1}{s}$
Adsorption	$5.2 \cdot 10^3$	$4.2 \cdot 10^3$
Reaction 1a	first TMA	$1.8 \cdot 10^7$
	second TMA	$2.1 \cdot 10^4$
	third TMA	7.3
	Gibbsite-surface	$1.9 \cdot 10^4$
Reaction 1b		$1.9 \cdot 10^6$
	Gibbsite-surface	$9.4 \cdot 10^2$
Reaction 1c	$0.4 \cdot 10^{-2}$	$4.4 \cdot 10^2$

$k_{1c} = 4.4 \cdot 10^2 \frac{1}{s}$, respectively. Since the free energy of adsorption of a single TMA molecule becomes positive above room temperature, the formation of the methyl-bridges is of importance during the adsorption process. The cooperative effect between the adsorbants may lead to an island like growth of the adsorbed layer. The reaction rates for the TMA-pulse reactions are presented in table 6.

The rate of the final ligand-exchange reaction is several magnitudes slower than the first two ligand-exchange reactions which

Table 5 Free energies of the reaction paths during the water pulse. Free energies are given in two temperatures, 450 K and 298 K (in parenthesis). Energy differences are taken with respect to the initial stage of the surface reaction. Adsorption energies are for a single adsorbed molecule. Values are given in eV.

Mechanism		ΔG_{ads}	ΔG_a	ΔG
Reaction 2a	(hydrogen bonded)	-0.05 (-0.65)	0.84 (0.84)	-1.56 (-0.90)
	(non-bonded)	0.51 (0.15)	0.28 (0.29)	-2.05 (-1.44)
Reaction 2b	(hydrogen bonded)	-0.19 (-0.81)	1.09 (1.09)	-1.09 (-0.44)
	(non-bonded)	0.18 (-0.42)	0.74 (0.72)	-1.61 (-0.98)
Reaction 2c	w1	0.72 (0.10)	0.30 (0.28)	-0.58 (-0.62)
	w2	0.62 (0.00)	0.64 (0.63)	-2.48 (-1.86)
	w3	0.81 (0.12)	0.23 (0.24)	-2.94 (-2.29)

Table 7 Reaction rate coefficients for different reaction pathways during the water pulse. Rate coefficients are given in temperatures 298 K and 450 K.

Mechanism	$k_{298}/\frac{1}{s}$	$k_{450}/\frac{1}{s}$
Adsorption	$1.4 \cdot 10^4$	$1.2 \cdot 10^4$
Reaction 2a (hydrogen bonded)	$3.9 \cdot 10^{-2}$	$3.9 \cdot 10^3$
(non-bonded)	$7.1 \cdot 10^7$	$7.2 \cdot 10^9$
Reaction 2b (hydrogen bonded)	$2.8 \cdot 10^{-6}$	6.2
(non-bonded)	4.2	$5.3 \cdot 10^4$
Reaction 2c w1	$1.2 \cdot 10^8$	$4.0 \cdot 10^9$
w2	$1.3 \cdot 10^2$	$6.5 \cdot 10^5$
w3	$4.8 \cdot 10^8$	$2.4 \cdot 10^{10}$

indicates that the main product from the TMA pulse is MMA. The production of MMA and methane consumes protons from the surface and turns hydroxyl groups into bare oxygen sites. These sites are very basic and can also adsorb TMA. As pointed out earlier in the text, the reaction barrier for the proton transfer between the lower and upper hydroxyl groups is only ca. 0.5–0.6 eV. Additional methane can be released when protons are transported from the lower hydroxyl groups to the previously reacted upper group oxygens. When all the protons on the surface have been consumed, the possible free oxygen sites are covered with new TMA. The formation of methyl-bridges between TMA and DMA/MMA can help stabilize the adsorbed molecules.

Similar kinetic parameters can be estimated also for the water pulse. The adsorption rate of water to the surface is $k_{\text{ads}} = 1.2 \cdot 10^4 \frac{1}{s}$ at the process conditions ($P = 2$ Pa, $T = 450$ K, with the empirical surface methyl-concentration of 5 Me/nm^2). The adsorption rate is larger for the water pulse than for the TMA pulse due to the smaller mass of the molecule and is of the same magnitude as some of the surface reactions. Several water molecules are likely to be present on the surface at the same time and the water–water interactions effect the energetics presented here, as can be seen in the case of mechanism **2c**. The interactions between the water molecules are likely to stabilize the transition states, so the estimations done using only one water molecule are give an upper bound for the reaction barriers. Reaction rates for the calculated pathways are presented in table 7.

While the reaction rates between the DMA and water are somewhat slow, the rates between water MMA are fast. This is essential as the MMA is estimated to be the main product of the TMA pulse. Overall the process is shown to be thermodynamically stable with negative free energy and to have reaction barriers that are accessible in the process conditions.

5 Conclusion

Density functional calculations for the initial surface reactions of the trimethylaluminium–water ALD-process are presented using a more realistic surface model than previously used in the literature. Several reaction pathways were searched and calculations include finite temperature effects.

TMA is found to adsorb exothermically. The overall reactions have very negative Gibbs free energy. The reaction barriers for the initial ligand-exchange reactions between the upper hydroxyl groups and the TMA were found to be small. TMA dissociation is predicted to terminate at monomethylaluminium. After the higher hydroxyl groups have reacted into MMA, the surface is left with bare oxygen sites and some remaining hydroxyl sites that are still susceptible to TMA adsorption and dissociation. This will lead to some DMA surface species. We predict that a methyl-bridge network is formed during the adsorption of TMA and is used to stabilize the adsorbed aluminium atoms at the end of the pulse.

Water pulse was studied using few water molecules. Water molecules were found to adsorb exothermically to DMA but adsorption to MMA has a small barrier. Reaction barriers with the main product from the TMA pulse, the MMA, are accessible in the process conditions. Single water molecule calculations with the DMA produced rather large barriers. However, static calculations with few water molecules were shown to be sensitive to water–water-interactions. Due to the fact that the adsorption rate if of the same order of magnitude as some of the surface reactions, the water–water-interactions probably play an important part in the dynamics of the surface reactions.

The TMA/H₂O system is one of the most studied ALD-processes, mainly experimentally. The surface processes are complex and difficult to measure but with computational research it is possible to obtain insight on the possible surface mechanisms and energetics. Understanding the surface processes and kinetics is essential in the design and optimization of ALD processes.

Notes and references

- 1 N. Pinna and M. Knez, *Atomic Layer Deposition of Nanostructured Materials*, Wiley-VCH, 2012.
- 2 M. Leskelä and M. Ritala, *Thin solid films*, 2002, **409**, 138–146.
- 3 S. M. George, *Chemical reviews*, 2009, **110**, 111–131.
- 4 R. Puurunen, *Journal of Applied Physics*, 2005, **97**, 121301.
- 5 M. Ritala and J. Niinistö, *ECS Transactions*, 2009, **25**, 641–652.
- 6 E. Gusev, M. Copel, E. Cartier, I. Baumvol, C. Krug and M. Gribyuk, *Applied Physics Letters*, 2000, **76**, 176–178.
- 7 D. Ha, D. Shin, G.-H. Koh, J. Lee, S. Lee, Y.-S. Ahn, H. Jeong, T.-Y. Chung and K. Kim, *Electron Devices, IEEE Transactions on*, 2000, **47**, 1499–1506.
- 8 A. Paranjpe, S. Gopinath, T. Omstead and R. Bubber, *Journal of the Electrochemical Society*, 2001, **148**, G465–G471.
- 9 R. Puurunen, M. Lindblad, A. Root and A. Krause, *Physical Chemistry Chemical Physics*, 2001, **3**, 1093–1102.
- 10 Y. Widjaja and C. Musgrave, *Applied Physics Letters*, 2002, **80**, pp. 3304–3306.
- 11 A. Heyman and C. B. Musgrave, *The Journal of Physical Chemistry B*, 2004, **108**, 5718–5725.
- 12 S. D. Elliott and J. C. Greer, *Journal of Materials Chemistry*, 2004, **14**, pp. 3246–3250.
- 13 S. D. Elliott and H. P. Pinto, *Journal of electroceramics*, 2004,

- 13, pp. 117–120.
- 14 S. Elliott, *Advanced Short-time Thermal Processing for Si-based CMOS Devices: Proceedings of the International Symposium*, 2003.
- 15 Z. Lodziana, J. Norskov and P. Stoltze, *Journal of Chemical Physics*, 2003, **118**, pp. 11179–11188.
- 16 J. e. Enkovaara, *Journal of Physics: Condensed Matter*, 2010, **22**, 253202.
- 17 J. P. Perdew, K. Burke and M. Ernzerhof, *Physical Review Letters*, 1996, **77**, p. 3865.
- 18 A. Tkatchenko and M. Scheffler, *Physical review letters*, 2009, **102**, 073005.
- 19 R. Bader, S. Anderson and A. Duke, *Journal of the American Chemical Society*, 1979, **101**, 1389–1395.
- 20 C. J. Cramer, *Essentials of computational chemistry: theories and models*, John Wiley & Sons, 2013.
- 21 P. W. Atkins and J. De Paula, *Oxford University Press, Oxford*, 2010, **917**, year.
- 22 G. Henkelman, B. P. Uberuaga and H. Jónsson, *The Journal of Chemical Physics*, 2000, **113**, 9901–9904.
- 23 S. D. Elliott, *Electrochem.Soc.Proc.Vol*, 2003, **14**, p. 231.
- 24 S. D. Elliott, *Computational materials science*, 2005, **33**, pp. 20–25.
- 25 A. Marmier and S. C. Parker, *Physical Review B*, 2004, **69**, 115409.
- 26 J. Guo, D. Ellis and D. Lam, *Physical Review B*, 1992, **45**, s. 13647.
- 27 X.-G. Wang, A. Chaka and M. Scheffler, *Physical Review Letters*, 2000, **84**, s. 3650.
- 28 R. D. Felice and J. Northrup, *Physical Review B*, 1999, **60**, R16287–R16290.
- 29 J. A. Kelber, *Surface science reports*, 2007, **62**, 271–303.
- 30 A. W. Ott, J. W. Klaus, J. M. Johnson and S. M. George, *Thin Solid Films*, 2009, **517**, 5950–5950.
- 31 It is unclear from the article whether or not the authors computed their results in the same manner. The results presented suggest that this is the case, however this is not clear from the text itself.
- 32 L. W. Finger and R. M. Hazen, *Journal of Applied Physics*, 1978, **49**, 5823–5826.
- 33 A. B. Mukhopadhyay, C. B. Musgrave and J. F. Sanz, *Journal of the American Chemical Society*, 2008, **130**, 11996–12006.